Turning a Digital Camera into an Absolute 2D Tele-Colorimeter

G. C. Guarnera[1], S. Bianco[2] and R. Schettini[2]

[1]NTNU - Norwegian University of Science and Technology, Gjøvik, Norway
[2]University of Milano-Bicocca, Milano, Italy

(a) Measured ground truth. (b) Our estimates. (c) Color difference, amplified by 2. (d) Comparison for the color chart.

Figure 1: In (a), XYZ values (in cd/m^2) measured with a 2D Color Analyzer under the D65 illuminant. In (b), XYZ values estimated by our system, in cd/m^2. For visualization, the XYZ values in (a) and (b) are converted into gamma corrected sRGB values. In (c), color difference in the sRGB space, amplified by 2. In (d), comparison for the color chart in the scene. The background of each square shows the ground truth and the circles at the center of each square, not always visible, show our estimates. The Normalized Root Mean Square Errors on the X, Y and Z channels are respectively 1.28%, 1.19% and 1.75%.

Abstract

We present a simple and effective technique for absolute colorimetric camera characterization, invariant to changes in exposure/aperture and scene irradiance, suitable in a wide range of applications including image-based reflectance measurements, spectral prefiltering and spectral upsampling for rendering, to improve color accuracy in HDR imaging. Our method requires a limited number of acquisitions, an off-the-shelf target and a commonly available projector, used as a controllable light source, other than the reflected radiance to be known.
The characterized camera can be effectively used as a 2D tele-colorimeter, providing the user with an accurate estimate of the distribution of luminance and chromaticity in a scene, without requiring explicit knowledge of the incident lighting power spectra. We validate the approach by comparing our estimated absolute tristimulus values (XYZ data in cd/m^2) with the measurements of a professional 2D tele-colorimeter, for a set of scenes with complex geometry, spatially varying reflectance and light sources with very different spectral power distribution.

Categories and Subject Descriptors (according to ACM CCS): I.3.3 [Computer Graphics]: Picture/Image Generation—I.4.1 [Image Processing and Computer Vision]: Digitization and Image Capture—I.4.8 [Image Processing and Computer Vision]: Scene Analysis—

1. Introduction

Digital reproduction of objects and scenes is still a challenge in Computer Graphics, with the ultimate goal to render images which are not distinguishable from pictures of the real world counterpart, under the same lighting and viewing conditions.

Radiometric functions such as BRDF [NRH*77], SVBRDF and BTF [DvGNK99] are commonly used to represent the appearance of many classes of materials, increasing the photo-realism of renderings. Measuring the reflectance properties of a material is potentially expensive and time consuming, in particular using ad hoc devices such as gonio-reflectometers [TS67, HR76, Foo97].

In recent years image-based measurement devices have become popular [MWL*99, DHT*00, MGW01, MPBM03, HP03, NDM05, RMS*08, FCM*08, GCP*09, GCP*10, GPDG12, RPG16, GHCG17], since they speed up reflectance measurements and

lower costs, by making use of a series of photographs of a material and mainly requiring off-the-shelf components; for a recent survey on reflectance representation and acquisition we refer the reader to a recent, comprehensive survey [GGG*16]. However, by using digital cameras instead of spectro-radiometers some issues arise, related to the typical design of consumer camera sensors.

In digital photography, photons incident on the sensor cause charge to accumulate at each pixel location, thus forming a picture. In loose analogy with the human visual system, camera sensors are equipped with a set of color filters that mimic the trichromatic color matching functions, generally mosaicing the captured image; the relation between the sensor irradiance and the RGB triplet is called Opto-Electronic Conversion Function (OECF). Consumer Digital Single Lens Reflex (DSLR) cameras are typically designed to produce aesthetically pleasing images, and obtaining good contrast and vivid colors is far more important than accurate colorimetric reproduction of the scene. Accordingly, specific designs of the spectral sensitivities of the color filter arrays are usually employed, thus affecting the way the sensor collects the charges and forms a RAW picture. A set of algorithms for demosaicing, white balancing, gamut mapping and color enhancement is subsequently applied, significantly modifying the initial sensor's output.

Given the above, in order to use a DSLR for color measurements, steps need to be taken to convert the acquired RGB values into meaningful radiometric and colorimetric data. The quality of the measurements can be assessed by standardized error formulas between the measured appearance and the original object [GLS04, GGG*16], such as the color difference metrics CIE ΔE^* [WS82], ΔE_{94} [CIEb] and CIEDE2000 [CIEc], easily derived from data in the CIE XYZ color space.

We propose an effective technique for DSLR characterization, able to measure physically accurate tristimulus values, requiring just a single, off-the-shelf target and a commonly available projector, used as a controllable light source to generate stimuli for the characterization. We break down the characterization task into two modules, the first one devoted to the absolute luminance estimation and the second one to the absolute colorimetric characterization. A camera characterized with our technique can be effectively used as a 2D tele-colorimeter, providing estimates of the absolute XYZ data in cd/m^2 even from a single shot; the accuracy of our method can be increased by acquiring an HDR sequence. Our estimates closely match the measurements of a professional instrument even on complex real-world scenes (figure 1, as confirmed by experimental results. Our technique can be used in image-based reflectance measurements, both in single and multiple view points setups (*e.g.*, BTF measurement domes), to provide accurate measurements for spectral prefiltering in rendering, to characterize HDR images and in general to increase the colorimetric accuracy of DSLR-based measurements.

In section 2 we provide a short summary of the possible applications in Computer Graphics, and discuss previous techniques for radiometric and colorimetric characterization, highlighting similarities and differences with our approach; a detailed description of our method is reported in section 3.

2. Background and Related work

In this work we focus on the sRGB colour space, defined in [ITU15], commonly used in cameras, monitor and HDTV, and on the CIE 1931 XYZ color space, the basis for color management systems, which contains all the colors perceived by humans. For a thorough review of color fundamentals we refer the reader to [WS82].

Color characterization of imaging devices establishes the relationship between the sensor responses to a set of colors and the corresponding colorimetric values. Various techniques have been proposed to find such a relationship, either requiring the acquisition of a reference color target (*e.g.*, a GretagMacbeth ColorChecker® [MMD76]) with known spectral reflectance [BSV09], or the use of specific equipment such as monochromators, as recommended by the standard ISO:17321-1:2006 [ISO06]. A characterized camera can be used in a range of different applications, which we review shortly before discussing previous techniques.

Reflectance Acquisition. The setup of a typical reflectance measurement device includes a light source to illuminate a portion of an object surface and a detector to measure how the light is scattered from the illuminated region. Gonioreflectometers offer high measurement accuracy, generally associated with high costs and long measurement times. Image-based reflectance measurement setups are aimed to lower costs and increase the throughput, measuring the light reflected from various surface orientations by taking a set of photographs [GGG*16]. Available designs range from single-camera devices, in which the light source is moved across a hemisphere of directions [MWL*99, MPBM03, NDM05] or make use of spherical illumination [GCP*10, GPDG12], to measurement domes, with tens or even hundred of cameras to observe the sample from different points of view [RMS*08]. In order to acquire meaningful data, performing a careful radiometric and colorimetric characterization of the cameras is of fundamental importance. Accurate color measurement instruments exist (*e.g.*, 2D colorimeters or spectro-radiometers), however their generally cumbersome design makes difficult to arrange them on a dome and they are quite expensive even for a single-camera setup, thus undermining some of the benefits offered by this class of acquisition setups.

HDR Characterization. High Dynamic Range (HDR) imaging makes possible to record real world scenes, where the dynamic range of luminance spans several orders of magnitude between bright and dark areas, without the loss of detail due to overexposed and underexposed pixels. Off-the-shelf digital cameras can be easily used to acquire radiance maps, suitable for image-based lighting techniques for instance, by combining multiple images acquired with different exposure times or aperture numbers into a single HDR image [DM97, MN99]; alternatively ad-hoc setups can be used, for instance by applying on the sensor a filter with spatially varying transmittance, such that adjacent pixels have different exposures [NM00]. Up to now, assessment of the radiometric accuracy of HDR images has mainly focused on the luminance, by solving the camera response function and mapping linearized pixel values to the scene radiance [RWPD05], whereas the colorimetric accuracy has received less attention [KK08], since most of

(a) (b) (c)

Figure 2: In (a), tristimulus values captured by the 2D Color Analyzer under the D65 illuminant, in cd/m^2, converted into the sRGB color space and gamma corrected. In (b) an HDR photograph of the same scene. In (c), the HDR image has been color balanced, taking advantage of the color checker depicted in the image. The color balancing has been performed using the HDR Shop built-in method [hdr]. In both (b) and (c) the depicted colors do not match the ground truth acquisition.

the available techniques are suited for Low Dynamic Range (LDR) images.

Spectral Prefiltering and Spectral Rendering. In order to achieve accurate color in photo-realistic rendering, a number of samples, equally spaced over the visible spectrum (*e.g.*, 5nm steps in the 380-780nm range as recommended in [CIEa]) must be taken into account, solving the rendering equation [Kaj86] by wavelength. As demonstrated by Meng *et al.* [MSHD15], employing the standard sRGB model in lighting calculation may cause color shifts, other than violations of the energy conservation principle. However, some practical barriers to applying spectral rendering still exist [WEV02, MSHD15]. To improve RGB rendering accuracy, Ward and Eydelberg-Vileshin [WEV02] proposed a simple Spectral Prefiltering method, which requires the knowledge of the spectral distribution of the dominant illuminant in the scene. Starting from a RGB texture depicting the reflected color of each surface, it applies a standard CIE formula to derive the corresponding XYZ colors, subsequently converted into white-balanced RGB color space for rendering. Meng *et al.* [MSHD15] proposed a fast method for spectral upsampling, which computes smooth spectra from XYZ tristimulus values, obtained from the input RGB textures; the recovered spectra can be used for spectral rendering, producing physically plausible images with reduced color artifacts. Other reflectance recovery methods in the state-of-the-art require in input XYZ values, used to recover plausible and smooth reflectance spectra, in the range $[0,1]$, perfectly metameric under a given illuminant [Bia10]. Therefore, the more faithful is the XYZ estimation, the more accurate is the recovered spectrum. In both spectral prefiltering and spectral upsampling techniques, a key step is the conversion into the XYZ color space of the input textures. Hence, photo-realistic rendering techniques can greatly benefit from our work, which provides accurate XYZ estimates of the input scene. Similar considerations can be done on illumination estimation.

Empirical DSLR characterization directly relates camera RGB data, from a photograph of a color target, to the measured colorimetric data. Many of these techniques are limited to linear regression on training samples, whereas more advanced methods use a white point preserving maximum ignorance assumption [FD97]. In figure 2 we report an example with HDR Shop v3.0 [hdr], which computes the transformation by creating a system of linear equations from each pixel channel, solved by finding the pseudo-inverse using SVD. Hubel *et al.* [HFHD97] compared several empirical techniques to compute the optimal 3×3 transformation matrix; such a class of approaches proves to be useful if the camera spectral sensitivities are unknown, under the assumption that the characterized camera will be used only in similar illumination conditions to those used for the characterization [Sha03]. The limited set of color patches on the target can lead to inaccurate results. Moreover, they are limited to low dynamic range imaging, since the intensity scale of the illuminant is discarded and only the relative spectral power distribution is preserved.

On the contrary, the aim of **absolute camera characterization** is to preserve the intensity scale, establishing a mapping between the captured RGB triplets and the absolute CIE-XYZ values, typically acquiring a set of pictures of scenes with known tristimulus values. Kim and Kautz [KK08] presented an ad-hoc transparent target, aimed to extend the applicability of characterization methods to HDR imaging, coupled with a D55 light source. Starting from an HDR sequence, they directly compute the XYZ values from the RGB values, using a 3x3 matrix derived through linear least-squares. There is a number of differences between our approach and the work by Kim and Kautz. The setups are very different, since we employ a white reflective target and a calibrated projector to emulate the Illuminant E and the tristimulus values of a standard color checker, allowing also for different possibilities. Rather than directly deriving the XYZ values from the RGB values, our approach makes use of two separate modules, aimed to preserve the absolute scale and to take into explicit account many factors simply embedded in the 3x3 matrix computed by [KK08]. We perform luminance characterization/estimation on single exposures, subsequently combined though exposure fusion; finally, we employ a very different strategy for the colorimetric characterization, performed through a pattern search.

Monochromator-based characterization approaches, in which a

white integrating sphere is illuminated with monochromatic light, prove to be accurate and of general application. The main drawback of monochromator-based techniques is the time required to collect the pictures of the sphere, which needs to be illuminated with a single wavelength at a time; moreover, the absolute scale for the luminance is absent [MVPC02]. Verdu *et al.* [MPVC03] describe an adaptation algorithm, aimed to obtain absolute measurements of a scene by exploiting the variation of the lens aperture or exposure time. It is the closest work to the algorithm we propose, however such similarities are purely due to the fact that both algorithms address the same problem, as highlighted in the following. The algorithm in [MPVC03] consists of spectral characterization, colorimetric characterization and linear correction. The spectral characterization requires a 250w Daylight lamp (D50) and a monochromator to estimate the Opto-Electronic Conversion Spectral Functions (OECSFs), used to derive the OECFs; we directly estimate the OECFs from our calibrated projector setup, which simulates the illuminant E with a high dynamic range; by inverting the OECFs we already have, at this stage, an estimation of the luminance in cd/m^2, equal to the true luminance Y if the incident illuminant is E. Concerning the colorimetric characterization, in [MPVC03] a light booth, equipped with the standard illuminants set (an incandescent lamp, a halogen lamp and a daylight lamp) and standard color checker (CC) are used; the ground truth is measured with a spectro-radiometer. From the measured data they estimate 4 different colorimetric profiles, either using least squares regression, or previous knowledge of the CC spectral reflectances, incorporated through autocorrelation matrix or Principal Component Analysis. Conversely, our colorimetric characterization relies on the aforementioned projector setup, which allows to modulate the relative and absolute spectral distribution of the light, thus removing the limitation to the standard illuminants; our colorimetric characterization matrix is computed through non-linear optimization, by means of a Pattern Search Method. In [MPVC03] an additional linear correction step is required, regardless of the colorimetric profile used, otherwise the absolute tristimulus values would be overestimated by one order of magnitude, as reported in their paper. Finally, although in [MPVC03] multiple exposure images are captured, only a single image with the best dynamic range for the scene is used, whereas we employ an exposure fusion algorithm. The details of our method are described in the following section.

3. Absolute Characterization of the DSLR Camera

The Red (R), Green (G) and Blue (B) pixel values of a raw RGB image, depicting a diffuse surface with spectral reflectance $S(\lambda)$, acquired under an illuminant with spectral power distribution $I(\lambda)$, by means of a camera sensor with spectral sensitivities $C_R(\lambda)$, $C_G(\lambda)$ and $C_B(\lambda)$, can be modeled as an integration over the visible part of the spectrum $\omega = [380-780]nm$ (equation 1). Similar expressions can be derived for the absolute CIE XYZ tristimulus values, as in equation 2, where $f_{\bar{x}}(\lambda)$, $f_{\bar{y}}(\lambda)$ and $f_{\bar{z}}(\lambda)$ are the CIE-1931 2-degree Color Matching Functions (*CMFs*):

$$\begin{cases} R \propto \int_\omega \mathrm{I}(\lambda)\mathrm{S}(\lambda)\mathrm{C_R}(\lambda)\mathrm{d}\lambda \\ G \propto \int_\omega \mathrm{I}(\lambda)\mathrm{S}(\lambda)\mathrm{C_G}(\lambda)\mathrm{d}\lambda \\ B \propto \int_\omega \mathrm{I}(\lambda)\mathrm{S}(\lambda)\mathrm{C_B}(\lambda)\mathrm{d}\lambda, \end{cases} \quad (1)$$

$$\begin{cases} X \propto \int_\omega \mathrm{I}(\lambda)\mathrm{S}(\lambda)\mathrm{f_{\bar{x}}}(\lambda)\mathrm{d}\lambda \\ Y \propto \int_\omega \mathrm{I}(\lambda)\mathrm{S}(\lambda)\mathrm{f_{\bar{y}}}(\lambda)\mathrm{d}\lambda \\ Z \propto \int_\omega \mathrm{I}(\lambda)\mathrm{S}(\lambda)\mathrm{f_{\bar{z}}}(\lambda)\mathrm{d}\lambda. \end{cases} \quad (2)$$

Comparing Eq.1 and Eq.2 it is clear that the only difference is the use of the *CMFs* instead of the sensor spectral sensitivities. In theory, a camera needs to satisfy Luther's condition in order to faithfully capture the colors of a scene:

$$\begin{bmatrix} f_{\bar{x}} \\ f_{\bar{y}} \\ f_{\bar{z}} \end{bmatrix} = M \cdot \begin{bmatrix} C_R \\ C_B \\ C_G \end{bmatrix}, \quad (3)$$

where M is a 3×3 matrix. In low-end cameras the Luther's condition holds only up to some extent, thus reducing their colorimetric accuracy.

In analogy with equation 3, we compute the estimated absolute tristimulus values through the following equation:

$$[X,Y,Z]^T cd/m^2 = \mathcal{M} \cdot \mathcal{T}\left([L(R),L(G),L(B)]\right)^T cd/m^2, \quad (4)$$

where $\mathcal{M}$ is the colorimetric characterization matrix, $\mathcal{T}$ is a polynomial transformation, and $L(R)$, $L(G)$, $L(B)$ are the luminance estimates obtained individually from each channel of the camera. A conceptually similar expression is commonly used in the context of ICC color profiles, known as shaper/matrix processing, to map into and from the Profile Connection Space (PCS), which generally is the XYZ color space [Sha03].

Pipeline Overview. The first module (subsection 3.1), models the OECFs from a sequence of equal tristimulus values reflected by a target and the corresponding raw RGB values acquired by the camera. In order to estimate the inverse OECFs, and obtain the absolute luminance $L(R|G|B)$ (equation 4), additional information is derived to normalize the raw pixel values, accounting for the actual sensor dynamic range, spectral sensitivities, and lens characteristics.

In general, the reflected tristimulus values are not all equal, due to non-uniform spectral power distribution of the illuminant, non-uniform spectral reflectance of the surface, or both. The second module is devoted to the colorimetric characterization of the camera/lens system (subsection 3.2), thus accounting for the general case. Some parameters, not explicitly modeled by the previous step, need to be handled (*e.g.*, spectrally dependent lens transmittance) and folded into the matrix $\mathcal{M}$ (equation 4). To derive $\mathcal{M}$, the module takes in input a sequence of non-uniform tristimulus values and the corresponding acquired RGB values, the latter used to estimate the luminance by the recovered inverse OECFs. With $L(R|G|B)$ and $\mathcal{M}$ at hand, equation 4 can be computed from the normalized pixel values, for any given input scene.

To achieve absolute characterization, measured RGB values must be related to a set of known radiance values, while preserving the intensity scale. Despite of this, as discussed in section 2, most reflectance-based techniques for camera characterization discard the intensity scale and are inherently low dynamic range, by making use of a gray-scale target, either real or simulated, illuminated by a known light source with fixed intensity. Moreover, previous works typically rely on a reflective color target, with a limited number of neutral and color patches, illuminated by an even narrower set of illuminants to derive the terms in equation 4 (see figure 3(a)). Hence, only a very sparse sampling of the possible incident lighting spectra and reflectance spectra is used for the characterization.

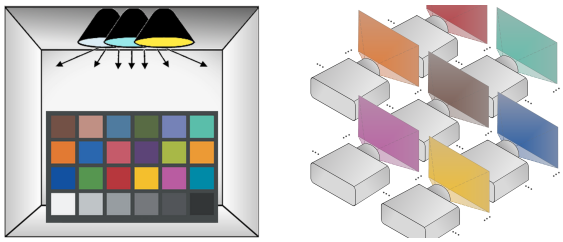

(a) (b)

Figure 3: In (a), typical color target and lighting booth setup. In (b), the proposed modulable light source (projector) setup.

In our work, we abandon the physical color target / light booth paradigm and make use of a characterized projector, acting as a controllable light source. The benefits such a core difference are dual fold:

- It allows to obtain approximately equal CIE XYZ tristimulus values (*i.e* $X = Y = Z$), with controllable intensity, which enables accurate modeling of the OECFs, without introducing any bias due to the combined effect of the light chromaticity and the channel-dependent sensor spectral sensitivities.
- Modulating the relative and absolute spectral distribution of the light beam, enables a virtually infinite number of illuminants to use for colorimetric characterization of the camera (figure 3(b)).

Such a freedom in designing $I(\lambda)$ (equations 1 and 2) allows to reduce the sampling in the space of the spectral reflectance $S(\lambda)$, even to a single spectrally neutral one. More important, it also removes any bias when the characterized camera is to be used in new lighting conditions.

3.1. Luminance estimation

In the following we assume that the reciprocity law holds for the system (camera and lens) to be characterized, *i.e.*, the sensor response depends only on the total exposure and, for instance, doubling the exposure time has the same effect of one stop increase in aperture or doubling the light intensity. Taking into account the OECFs $\mathcal{F}_R$, $\mathcal{F}_G$ and $\mathcal{F}_B$, the discrete representation of equation1, in a small area close to the optical axis, can be written as:

$$\begin{aligned} R &= \mathcal{F}_R\left(\frac{t}{N^2}\sum_{\lambda\in\omega} T(\lambda)I(\lambda)S(\lambda)C_R(\lambda)\triangle\lambda\right) \\ G &= \mathcal{F}_G\left(\frac{t}{N^2}\sum_{\lambda\in\omega} T(\lambda)I(\lambda)S(\lambda)C_G(\lambda)\triangle\lambda\right) \\ B &= \mathcal{F}_B\left(\frac{t}{N^2}\sum_{\lambda\in\omega} T(\lambda)I(\lambda)S(\lambda)C_B(\lambda)\triangle\lambda\right), \end{aligned} \tag{5}$$

where t is the exposure time, N is the f-number and $T(\lambda)$ is the lens transmittance, and $S(\lambda)$, $I(\lambda)$, $C_{R|G|B}(\lambda)$ are respectively the spectral reflectance of the surface, the spectral power distribution of the illuminant and the camera sensor with spectral sensitivities, as in eq. 1. In order to estimate the luminance Y we must derive the inverse OECFs $\mathcal{F}^{-1}_{R|G|B}$. The effectiveness of camera characterization can be limited by the limited dynamic range of the sensor, further reduced by the noise floor, assumed to be independent of the color channel, which acts as an additive term on equation 5: $R|G|B = \mathcal{F}_{R|G|B}(\cdot) + n$. Similarly to HDR imaging, the possibility to vary the exposure time or the lens aperture between two subsequent shots, can mitigate such a limitation, extending the measurement range of the system.

Given a sequence of tristimulus values $X_i = Y_i = Z_i$ reflected by a spectrally neutral target, with $i = 1,\ldots,\#_{stimuli}$, and the corresponding HDR photographs, for each pixel p_i, with coordinates $(u_{p_i}, v_{p_i}), 1 \le u_{p_i} \le U, 1 \le v_{p_i} \le V$ on the sensor lattice, we have:

$$[R|G|B]_{p_{i,t,N}} \propto \left[\mathcal{F}_{R|G|B}(T, Y_i, C_{R|G|B}, t, N)\right]_p + n, \tag{6}$$

since $Y = \sum_{\lambda\in\omega} I(\lambda)S(\lambda)\triangle\lambda$, under the hypothesis $X = Y = Z$.

Normalization. To be suitable for inverting the OECFs, the acquired raw RGB values must be normalized, accounting for a number of characteristics of real world devices.

- The actual range of useful digital values can be smaller than the theoretical maximum value given by the bit-depth J. In fact, on the low intensities side the noise floor n affects the minimum recorded value, whereas on the high intensities side the saturation value S can be smaller than $2^J - 1$. We estimate the noise floor n from a sequence of pictures acquired with the cap on the lens, at different times and averaging them.
- The CIE-CMFs have equal areas, whereas the areas beneath the sensor spectral sensitivity curves might differ from each other, thus affecting the measured RGB values. To estimate the sensor spectral sensitivity curves we used the technique described by Jiang *et al.* [JLGS13], which requires one additional picture of a reflective color target with known relative spectral reflectances (*e.g.*, a Color Checker®), acquired under daylight illumination. When an Equal Energy Illuminant is used, since the curves are fixed and do not vary with the exposure or the aperture, these factors can be embedded into constant terms, derived from the actual areas beneath $C_{R|G|B}(\lambda)$, denoted by $A_{R|G|B}$.
- Due to mechanical and optical properties of physical lenses, pixels away from the optical axis receive progressively less light as the distance increases, thus causing a radial variation in equation 5 (lens fall-off or vignetting). For each pixel, we relate its known radial distance from the center of the sensor to the average radial decrease in the acquired values (equation 6). A per pixel correction term is derived, and approximated with a 2^{nd} degree polynomial: $f(u_p, v_p) = p_1 r^2(u_p, v_p) + p_2 r(u_p, v_p) + p_3$; $r(u_p, v_p)$ is the radial distance of a pixel to the center $\{u_c, v_c\}$. $f(u_p, v_p)$ is equal to 1 for $(u_p, v_p) = (u_c, v_c)$.

By putting all together and dropping the subscripts, the normalization can be written as:

$$\begin{aligned} R' &= \frac{(R-n)A_G}{(S-n)A_R} f(u_p, v_p) \\ G' &= \frac{(G-n)}{(S-n)} f(u_p, v_p) \\ B' &= \frac{(B-n)A_G}{(S-n)A_B} f(u_p, v_p). \end{aligned} \tag{7}$$

To model the OECFs, the normalized values $\left[R', G', B'\right]_{i,t,N}$

are fitted to the corresponding known luminance values Y_i, $i = 1,\ldots,\#_{stimuli}$, for a given pair $\{t,N\}$. A different family of curves can be derived for each $\{t,N\}$, all parallel if the reciprocity law is verified. Ideally the amount of charge is a linear function of the sensor irradiance, hence a rather simple expression is a good candidate for fitting the OECFs, from which their inverse are easily derived:

$$\begin{aligned}\mathcal{F}_R^{-1}(R',t,N) &= \frac{R'^{\frac{1}{k_{3,R}}}}{k_{2,R}} - k_{1,R}\\ \mathcal{F}_G^{-1}(G',t,N) &= \frac{G'^{\frac{1}{k_{3,G}}}}{k_{2,G}} - k_{1,G}\\ \mathcal{F}_B^{-1}(B',t,N) &= \frac{B'^{\frac{1}{k_{3,B}}}}{k_{2,B}} - k_{1,B},\end{aligned} \tag{8}$$

where the constants $k_{1,R/G/B}$, $k_{2,R/G/B}$, and $k_{3,R/G/B}$ are derived by the fitting procedure and also absorb the transmittance $T(\lambda)$; $k_{1,R/G/B}$ account for the offset due to noise sources other than the noise floor, $k_{2,R/G/B}$ account for the absolute scale, whereas $k_{3,R/G/B}$ account for any residual non-linearity (gamma). By construction, if the reflected absolute tristimulus values are all equal $(X = Y = Z)$, then $\forall(p,t,N)$:

$$\mathcal{F}_R^{-1}\left(R',t,N\right) = \mathcal{F}_G^{-1}\left(G',t,N\right) = \mathcal{F}_B^{-1}\left(B',t,N\right) = Y\,cd/m^2. \tag{9}$$

The interval $S-n$ is subdivided into 3 disjoint intervals Z_u, Z_c and Z_o, whose widths depend on a parameter w, the latter accounting for the reliability of the pixel values towards the lower and upper bound of the normalized pixel range:

$$\begin{cases} Z_u = \left]n, \frac{(S-n)}{w}\right] \\ Z_c = \left]\frac{(S-n)}{w}, \frac{(w-1)(S-n)}{w}\right] \\ Z_o = \left]\frac{(w-1)(S-n)}{w}, (S-n)\right[\end{cases}.$$

A simple way to combine the luminance estimates from a series of photographs, acquired with a different exposure t , is described in algorithm 1, where $\{t_g,N_g\}$ is the initial guess. A similar algorithm can be described for the aperture selection, although it might require the use of several fall-off correction functions for the normalization, the fall-off being dependent on the aperture. Alternatively, a standard approach based on the work by Debevec and Malik [DM97] could be used.

In general, the illuminant spectral power distribution and the surface reflectance are not constant across the visible spectrum, causing the per channel estimates (equation 8) to differ from each other, while preserving the absolute scale of the tristimulus values. Hence, a different notation is used:

$$L(R|G|B)\,cd/m^2 = \mathcal{F}_{R|G|B}^{-1}\left(R'|G'|B',t,N\right). \tag{10}$$

The role of the colorimetric characterization, described in the next subsection, is to refine the output of equation 10 accounting for the general case, when also the spectrally dependent lens transmittance $T(\lambda)$ might contribute to deviations from equation 9.

3.2. Colorimetric Characterization

To derive the colorimetric characterization matrix $\mathcal{M}$ (equation 4), a set of spectrally non-uniform illuminants is projected on the white

Algorithm 1 Pseudo-code of a simple algorithm to estimate, for each pixel p with normalized values, the absolute luminance per channel (green, in the example). The luminance estimates from each channel are derived independently, using the same algorithm.

procedure ESTLUMINANCE(G'_{t_g,N_G},t_g,N_g)
  if $G'_{t_g,N_G} \in Z_c$ **then**
    $Luminance_p \leftarrow \mathcal{F}_G^{-1}\left(G'_{t_g,N_G},t_g,N_g\right)$
  else if $G'_{t_g,N_G} \in Z_u$ **then**
    $Luminance_p \leftarrow$ ESTLUMINANCE($G'_{2*t_g,N_G}, 2*t_g, N_g$);
  else
    $Luminance_p \leftarrow$ ESTLUMINANCE($G'_{\frac{t_g}{2},N_G}, \frac{t_g}{2}, N_g$);
  end if
  return $Luminance_p$
end procedure

reflective patch. The corresponding ground truth tristimulus values, and the $L(R|G|B)$ estimated by equation 10, are used in the following optimization problem [BGRS07]:

$$\mathcal{M} = \arg\left(\min_{M\in\mathbb{R}^{3\times P}} median(E) + mean(E) + max(E)\right), \tag{11}$$

$$E = \left|\left|[X,Y,Z]^T - M\cdot\mathcal{T}([L(R),L(G),L(B)])^T\right|\right|_1, \tag{12}$$

where $||\cdot||_1$ denotes the L_1 norm, $\mathcal{T}$ is a polynomial transformation to be applied to the estimated $L(R|G|B)$ values, and P is the number of polynomial terms given in output by $\mathcal{T}$. In this work, following [BS14], three different kinds of transformation $\mathcal{T}$ have been taken into account. The first one is the identity, so that the color correction is done with linear polynomial:

$$\mathcal{T}_1(L(R|G|B)) = [L(R),L(G),L(B)]. \tag{13}$$

The second one is the linear polynomial with an offset term:

$$\mathcal{T}_o(L(R|G|B)) = [L(R),L(G),L(B),1]. \tag{14}$$

The third one is the second order rooted polynomial [FMH11]:

$$\begin{aligned}\mathcal{T}_{2R}(L(R|G|B)) = [&L(R),L(G),L(B),\\ &\sqrt{L(R)L(G)},\sqrt{L(R)L(B)},\sqrt{L(G)L(B)}].\end{aligned} \tag{15}$$

Since the objective function is non-linear and non-differentiable, the optimization problem is solved using the Pattern Search Method (PSM). PSMs are a class of direct search methods for nonlinear optimization [LT00]. PSMs are simple to implement and do not require any explicit estimate of derivatives. Furthermore, global convergence can be established under certain regularity assumptions of the function to minimize [LT97]. The general form of a PSM is reported in Algorithm 2, where f is the function to be minimized, k is the iteration number, x_k is the current best solution, D_k is the set of search directions, and Δ_k is a step-length parameter.

Once the colorimetric characterization matrix $\mathcal{M}$ has been found, the characterization is complete and the estimate of the absolute tristimulus values can be obtained using equation 4.

Algorithm 2 Pseudo-code of the general form of a pattern search method (PSM).

while $\Delta_k >$ thresh and $k <$ maximum iteration number **do**
  for each $d_k \in D_k$ **do**
    $x^* \leftarrow x_k + \Delta_k d_k$
    if $\exists d_k \in D_k : f(x^*) < f(x_k)$ **then**
      $x_{k+1} \leftarrow x^*$
      $\Delta_{k+1} \leftarrow \alpha_k \Delta_k$ with $\alpha_k > 1$
    else
      $x_{k+1} \leftarrow x_k$
      $\Delta_{k+1} \leftarrow \beta_k \Delta_k$ with $\beta_k < 1$
    end if
  end for
  $k \leftarrow k+1$
end while

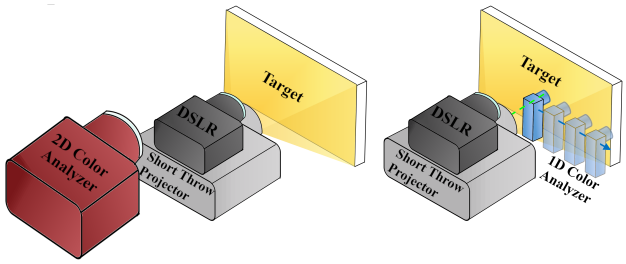

(a) 2D Color Analyzer setup. (b) 1D Colorimeter setup.

Figure 4: Proposed setup for absolute camera characterization.

4. Experimental Setup

A schematic representation of our setup is reported in figure 4(a). A Canon 40D camera with a standard $28-135mm$ $f/3.5-5.6$ zoom lens is used in this work; the focal length is set to $30mm$. The lens f-number ranges from $f/4$ to $f/22$, on a standard full-stop scale. To reduce stray light, and increase the accuracy, a slip-on lens hood is used. The camera sensor is equipped with a standard color filter array, thus reducing the spatial resolution in each color channel (sampling factor of $1:2$ for the Green and $1:4$ for both the Red and Blue values). The ISO setting is fixed to the native value of the sensor (ISO 100).

As reflective target an A4-format white diffuse patch is used, consisting of a white uncoated professional photo paper without bleaching (alternatively, the ColorChecker®White Balance Card could be used). The reflective target is fixed to a blackboard placed in front of the projector, roughly at the center of the light beam, about 0.6m away from it. The target is roughly lambertian, hence, thanks to the alignment with the projector, the surface reflectance varies smoothly. A simple interpolation, performed individually for each channel, proves to be sufficient to handle the reduced spatial resolution of the camera sensor due to the color filter array.

A Dell S300 DLP projector, with a maximum brightness of 2200 ANSI lumens, is aligned with the camera and employed as controllable light source. The projector calibration involved the use of a X-Rite *i1Pro2* spectro-photometer, to correct for the gamma and to obtain an equal tristimulus scale.

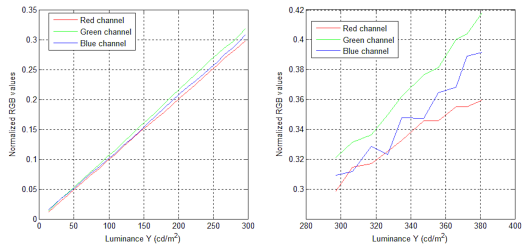

(a) (b)

Figure 5: (a) Sensor response (OECFs) estimated from the normalized raw RGB values; the illuminant in the scene has equal tristimulus values. (b) Sensor response measured using an illuminant with slightly perturbed tristimulus values w.r.t. a neutral value.

A *KonicaMinolta CA* $-$ 2500 2D Color Analyzer, equipped with a XYZ color filter, is used for the system characterization and to obtain the ground truth in our experiments. The resolution of the instrument is 980×980 pixels, and the luminance measurement range is $0.1-100000\,cd/m^2$. The DSLR camera is aligned with the light beam, with the white patch placed in the middle of the image formation plane, in order to allow the estimation of the lens fall-off. Please note that to characterize the DSLR, and estimate the fall-off, luminance and chrominance measurements could be obtained in different ways, for instance using the aforementioned *i1Pro2* and taking a set of measurements along the radial direction from the center of the light beam (figure 4(b)); in our experiments we also demonstrate this option. Additionally, the ground truth could be estimated from the known spectral reflectance of the diffuse patch $S(\lambda)$ and the spectra of the projected light $I(\lambda)$.

Luminance Training Set. To train the luminance estimation module, the projected light beams have the same relative spectral distribution and different absolute intensity. The luminance Y on the reflective target is varied in the range $0-890\,cd/m^2$, with steps of about $30\,cd/m^2$. For each reflected equal tristimulus value, a sequence of pictures of the reflective target is acquired, as described in section 3.1. All images are saved as RAW files, with no debayering nor white balancing. Figure 5 helps understanding the importance of using a controllable Equal Energy Illuminant, in our setup implemented through a calibrated projector, and of the normalization. The normalized $[R',G',B']$ values are plotted versus the ground truth luminance Y, for a fixed f-number and shutter time t. As figure 5(a) shows, the response is almost linear ($k_{3,R/G/B} \approx 1$ in our experiments). In figure 5(b) the same settings for the lens and camera are used, whereas the tristimulus values X and Z of the projected light are obtained by applying small random perturbations to the Y value, in the range $X,Z = Y \pm 5\%$. Since the sensor response is no longer linear, to describe the inverse OECFs a more complex expression than equation 8 would be required. Not accounting for the terms $A_{R|G|B}$ in equation 7, linearly correcting the normalized RGB values, would lead to a change in the slopes of the curves reported in figure 5(a), which could sensibly differ from each other; to enforce equation 9 the different slopes would be folded into $k_{2,R/G/B}$, ultimately affecting the performance of the colorimetric characterization.

Figure 6: The 24 photographs of the colored patches used for the colorimetric characterization, obtained by projecting the XYZ tristimulus values of a standard color checker on the reflective target.

Figure 7: Some of the flat color targets used in Experiment (a) and (c), placed on a magnetic blackboard (on the background).

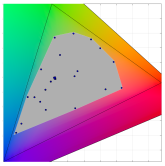

Training set for colorimetric characterization. The same setup is used to project on the target a set of light beams with different chromaticity, from which the matrix $\mathcal{M}$ (section 3.2) is derived. To fairly compare with previous methods [BSV09, MPVC03], and at the same time to reduce the number of acquisitions, in this work we limit the characterization set to the 24 illuminants which reflected by the target produce the XYZ values of a physical ColorChecker® (figure 6), and demonstrate that they suffice to outperform prior art. Such a choice limits the colors available for the characterization to a subset of the color space of the projector, namely sRGB (grey area of the inset; the black triangle encloses the sRGB chromaticity). While the 24 patches could be combined in a single projected image, this would reduce the physical area of each patch on the A4 target. Hence, the ground truth data available would be reduced, as well as the camera RGB data on the acquired images, further affected by sampling due to the Bayer pattern and by the edge spread, due to surface roughness of the target; it would also introduce a dependency on the location of each patch, due to the lens fall-off for instance, thus requiring a more complex processing.

Experiments and Test Sets. We performed two different sets of experiments with the camera characterized with the $CA-2500$ setup. The first set makes use of a similar setup to the camera characterization one, with the white diffuse target being in turn replaced by a color target, selected from a set of 8 different ones with non-uniform spectral reflectances (figure 7). Each target is illuminated by a set of 30 illuminants, with different spectral power distribution, thus obtaining 8×30 samples (*Experiment (a)*).

As for the second set of experiments, we acquired a complex scene with several objects placed inside a Macbeth "The Judge" Portable Light Viewing Booth. The set of objects includes, other than a standard color checker, plushies, metal and plastic toys, with very different geometries, colors and reflectance properties. In turn, three different illuminants have been used in the scene: a standard CIE D65 (noon daylight - D65), CIE F2 (Cool White Fluorescent - CWF) and CIE A (Incandescent Light Source - ILS). For each illuminant we simulated and additional condition, by partially occluding the illuminant itself, thus increasing the spatial variation of the irradiance; in total we acquired 3×2 complex scenes (*Experiment (b)*). The scenes have been acquired at the same time by the camera and the Color Analyzer; for practical reasons, the optical axis of the camera and of the color analyser are not perfectly aligned. To account for the slight misalignment and the different resolutions of the two devices, the acquired color measurements have been warped to the photographs, using the non-rigid registration algorithm by Rueckert *et al.* [RSH*99]. The photographs of the booth scene are reported in figure 8, whereas figure 9 shows the differences between the scene as seen by the camera and by the Color Analyzer. Overall, such a set of experiments allows to assess the robustness of the proposed method to complex reflectances, uneven illumination and the capability to estimate colors beyond the sRGB color space used for the characterization, a common case in real world scenes.

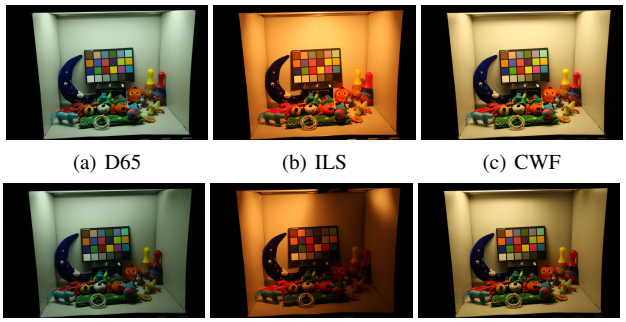

(a) D65 (b) ILS (c) CWF

(d) D65, partly covered (e) ILS, partly covered (f) CWF, partly covered

Figure 8: Experiment (b) - Photographs of the test scenes inside the lighting booth, under different illuminants.

Table 1: White points of the booth scenes (see Figure 8), in cd/m^2.

Scene	X	Y	Z
D65	213.84	225.00	244.98
D65, partly covered	146.36	154.00	167.68
ILS	1751.01	1594.00	567.15
ILS, partly covered	441.60	402.00	143.03
CWF	298.04	320.00	174.34
CWF, partly covered	167.89	180.34	97.68

We performed an additional experiment (*Experiment (c)*), in which the X-Rite *i1Pro2* Spectrophotometer is used to characterize the camera, with the same procedure described for the $CA-2500$ and accounting for the different specifics of the instrument, which provides measurements limited to an average over a small area. The test set consists of a sequence of 27 RGB values projected on 4 different colored targets, for a total of 108 measurements. The RGB values are selected by ensuring that no reflected XYZ value belongs to the training set (see figure 13(b)).

(a) (b)

Figure 9: Booth scene as seen by the camera (a) and by the 2D Color Analyzer (b).

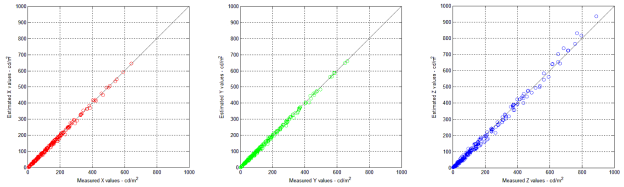

Figure 10: Estimated absolute tristimulus values versus the ground truth. All measures are in cd/m^2.

4.1. Results and Discussion

To evaluate the accuracy of the proposed characterization we computed the ΔE_{94} [CIEb] and the $CIEDE2000$ (ΔE_{00}) [CIEc] color differences between our estimated absolute tristimulus values and the ground-truth. To compute the color differences all values must be converted into the $CIELab$ color space, hence a white point must be selected [WS82].

White point selection. As for Experiments (a) and (c), the white point W_r is set to the Equal Energy Illuminant E, with $X_E = Y_E = Z_E = 890 cd/m^2$, the maximum ground truth luminance in this setup. As for Experiments (b), for each illuminant in the booth, the reference white point $W_r = [X_r, Y_r, Z_r]$ is set to the XYZ values of the white patch of the color checker $W_w = [X_w, Y_w, Z_w]$, linearly scaled to the maximum luminance value observed in the scene, thus preserving the actual chromaticity (see table 1). In fact, due to the geometry of the booth and the placement of the objects inside it, some regions Q of the booth itself are brighter than the white patch, with $Y_Q \gg Y_w$; hence, we set W_r to:

$$W_r = \left[X_w \frac{Y_Q}{Y_w}, Y_Q, Z_w \frac{Y_Q}{Y_w} \right] cd/m^2. \quad (16)$$

Experiment (a) In Table 2 we report the differences computed for both the training and the test sets using the simplest transformation for the colorimetric profile ($\mathcal{T}_1$, in equation 13); in figure 10 the estimated X, Y and Z values for the test set are plotted versus their respective ground truths. In particular, on the luminance Y the relative error is 2.37%, and the median absolute error is 2.7 cd/m^2. Results with the other two transformations for the colorimetric profile, defined in section 3.2, are not reported since statistically equivalent to those reported in Table 2.

Experiment (b) In figure 11 we report the area of the chromaticity diagram occupied by the test scene in the lighting booth, as seen under each of the selected illuminants; the (x, y) chromaticities are derived as $x = X/(X+Y+Z)$ and $y = Y/(X+Y+Z)$. As the diagrams clearly show, the color range of these scenes is beyond the sRGB color space used for the characterization. In table 3 we report a summary of the statistics about the measured ΔE_{94} and ΔE_{00} errors on the booth scenes, using either a single or multiple shots; table 4 reports the Normalized Root Mean Square Error (NRMSE) for each scene. Figure 12 shows the ΔE_{94} and ΔE_{00} error maps for the scene captured under the D65 illuminant, partly covered. The highest errors are localized around the edges of the objects, probably introduced by the non-rigid registration (see figure 12(b) and 12(e)). By clamping the error map to the maximum value measured in a non-edge area, a better visualization of the error due to the technique itself can be obtained (figures 12(c) and 12(f)). Despite of the slight misalignment between camera and Color Analyzer, our results clearly show the robustness of the proposed approach.

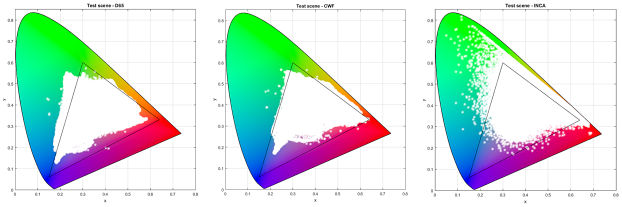

Figure 11: Chromaticity of the test scenes used in Experiment (b). The chromaticity of the sRGB color space, used for the characterization, is enclosed in the black triangle. From left to right, chromaticity of the scene under the D65, CWF and ILS illuminants.

Table 2: Experiment (a). Color accuracy using the transformation $\mathcal{T}_1$ for the colorimetric profile (see equation 13) and a single shot.

	ΔE_{94}				ΔE_{00}			
	min	median	mean	max	min	median	mean	max
Training	0.2514	0.6703	0.7213	1.7659	0.2853	0.7228	0.7434	2.2197
Test	0.0618	1.7428	1.7622	3.9997	0.0617	1.6317	1.6352	4.5783

Experiment (c) Figure 13 visually summarizes the outcome of the $i1Pro2$ experiment. In figure 13(a) we report the XYZ values used as training set (background of each square) and our estimates (the circles at the center of each square); the differences are not visible or barely visible. Figure 13(c)- 13(f) show the reflected values obtained by projecting the RGB values in figure 13(b) respectively on a white target and on the 3 leftmost colored target in figure 7; please compare the background of each square (ground truth) with the circle at its center (our estimates). Table 5 reports the numerical evaluation of the errors, showing that the NRMSE is at most 3% and the colorimetric errors ΔE_{94} and ΔE_{00} are lower than 2.

5. Conclusions

We presented a simple and effective technique for absolute colorimetric camera characterization. The characterized camera can be effectively used as a 2D tele-colorimeter, providing the user with an accurate estimate of the luminance and chromaticity distribution in a scene (absolute XYZ tristimulus values in cd/m^2). The

Table 3: Experiment (b) (booth scenes), color accuracy. The single-shot images have been acquired at $(f/8, 0.4s)$; the multiple shot estimates are derived from 3 exposures. The statistics computed including the edge areas are reported between parenthesis. The results refer to the colorimetric profile derived from equation 15, which overall provides the most accurate estimates. The colorimetric profile from equation 14 provides comparable results for the illuminant ILS.

	ΔE_{94}				ΔE_{00}			
	min	median	mean	max	min	median	mean	max
D65, single shot	0.0114	1.8079 (2.1376)	3.0498 (3.6719)	10.8743 (47.6062)	0.0116	1.4515 (1.9515)	2.3650 (3.4129)	8.7549 (49.4036)
D65, multiple shot	0.0769	1.4844 (1.7516)	2.4152 (3.0214)	9.4572 (44.0365)	0.0077	1.2731 (1.5766)	2.0581 (2.7960)	8.2894 (47.4557)
D65 partly covered, single shot	0.0452	2.4160 (2.4793)	3.2249 (3.5977)	10.1600 (65.6070)	0.0410	2.2516 (2.3408)	3.0126 (3.4731)	8.2601 (43.8293)
D65 partly covered, multiple shot	0.0199	2.1925 (2.2372)	2.8198 (3.1821)	8.799 (64.8081)	0.0161	2.0443 (2.1156)	2.5636 (3.0177)	7.349 (40.4064)
ILS, single shot	0.0000	2.2595 (2.5266)	2.8006 (3.6991)	8.0393 (51.1465)	0.0000	2.8368 (3.0840)	3.3098 (4.0892)	8.4848 (47.2321)
ILS, multiple shot	0.0000	2.0524 (2.2168)	2.5414 (2.8572)	7.7342 (37.6484)	0.0000	2.5255 (2.6658)	2.9773 (3.2634)	8.2642 (34.0391)
ILS, partly covered, single shot	0.0000	2.1976 (2.2709)	2.6088 (2.8939)	8.5903 (71.3605)	0.0000	2.3944 (2.4982)	2.7578 (3.0962)	7.1160 (47.0875)
ILS, partly covered, multiple shot	0.0000	1.9047 (1.9713)	2.3042 (2.5430)	7.8434 (45.7118)	0.000	2.0877 (2.1641)	2.4720 (2.7101)	6.9269 (45.9015)
CWF, single shot	0.0034	3.1048 (3.4127)	4.3133 (5.3696)	18.8155 (84.4061)	0.0045	2.5169 (2.8145)	3.8778 (4.7634)	18.8421 (63.3275)
CWF, multiple shot	0.0034	2.6768 (2.9075)	3.6685 (4.3942)	18.6554 (73.2726)	0.0045	2.1674 (2.3572)	3.0521 (3.8445)	14.0870 (54.4615)
CWF, partly covered, single shot	0.0117	2.1776 (2.8921)	3.7476 (4.8132)	15.1012 (60.1606)	0.0112	2.1273 (2.6958)	3.3060 (4.4174)	12.0586 (52.0676)
CWF, partly covered, multiple shot	0.0084	1.6927 (2.0604)	2.8992 (3.6049)	14.2131 (58.9830)	0.0112	1.6192 (2.0197)	2.5724 (3.3283)	10.9125 (49.9891)

Table 4: NRMSE for the test scenes in the light booth.

	Single shot			Multiple shot		
Scene	X	Y	Z	X	Y	Z
D65	0.0136	0.0131	0.0189	0.0128	0.0119	0.0175
D65, partly covered	0.0165	0.0174	0.0176	0.0119	0.0120	0.0133
ILS	0.0110	0.0104	0.0125	0.0070	0.0064	0.0091
ILS, partly covered	0.0197	0.0172	0.0170	0.0127	0.0117	0.0210
CWF	0.0177	0.0164	0.0209	0.0151	0.0141	0.0183
CWF, partly covered	0.0141	0.0138	0.0155	0.0110	0.0105	0.0131
Average	0.0154	0.0147	0.0171	0.0117	0.0111	0.0154

Table 5: NRMSE, ΔE_{94} and ΔE_{00} for the *i1Pro2* experiment.

	NRMSE			Colorimetric Error	
Reflective Target	X	Y	Z	ΔE_{94} (mean)	ΔE_{00} (mean)
White	0.0046	0.0057	0.0131	1.2056	1.1444
Yellow	0.0057	0.0078	0.0281	1.9324	1.8155
Pink	0.0161	0.0218	0.0262	1.6385	1.5055
Light Blue	0.0146	0.0067	0.0296	1.5567	1.3803

efficacy of our approach is demonstrated comparing the estimated absolute tristimulus values with the measurements of a professional 2D Color Analyzer for a set of scenes with complex geometry, spatially varying reflectance and light sources with very different spectral power distributions. Experimental results show that our method is able to estimate the absolute XYZ tristimulus values of complex scenes with an average NRMSE of less than 1.6% when a single photograph is used, and less than 1.3% using multiple exposures. Additionally, we demonstrate that even a 1D spectrophotometer can be used for the characterization or, equivalently, a camera characterized with our method could replace this instrument for XYZ measurement, with the advantage of providing 2D measurements.

The proposed method is suitable for use in a wide range of applications, including image-based measurements of reflectance [GGG*16]; in rendering, to provide accurate input data for spectral prefiltering and spectral upsampling of input textures; additional applications include characterization of HDR imaging [KK08], to provide more accurate illumination estimation [Deb98, LYL*16], and in augmented and mixed reality applications [RPAC17]. Industrial applications include the use as an analysis tool to compare the raw performance of commercial cameras [MPVC03]; in colorimetry, to perform color characterization of displays and projectors, and in general the absolute measurement of non-homogeneous samples, given the possibility of simultaneously measuring the whole visual field. As future work we plan to investigate the applicability of the proposed technique to more complex processing pipelines [BBNS12, BBNS13].

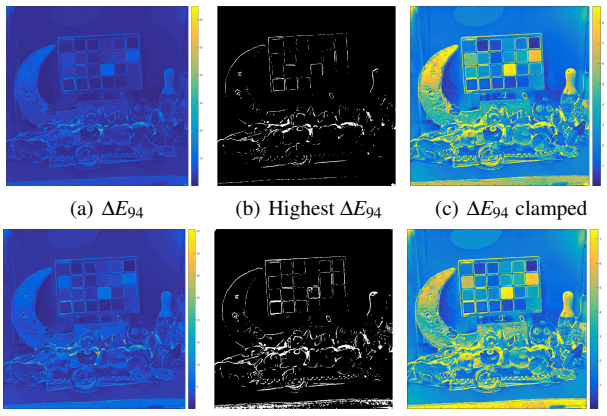

(a) ΔE_{94} (b) Highest ΔE_{94} (c) ΔE_{94} clamped

(d) ΔE_{00} (e) Highest ΔE_{00} (f) ΔE_{00} clamped

Figure 12: Error maps of the booth scene, under the D65 partly covered. The edges of the objects have the highest errors.

Acknowledgments

We thank the anonymous reviewers for suggestions on improving this manuscript. We also wish to thank Marco Buzzelli for help with data acquisition and Dar'ya Guarnera for assistance with figures. Maurizio Rossi provided us with the 2D color analyzer used for ground truth measurements. This work was partially supported by

the MUVApp project N-250293, funded by the Research Council of Norway.

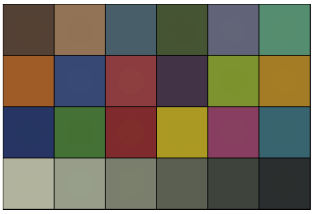

(a) Training Set

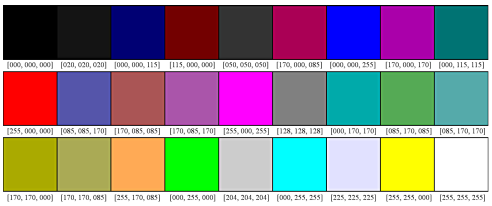

(b) Projected RGB values for the test set

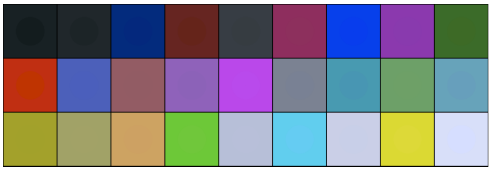

(c) Reflected values - white surface

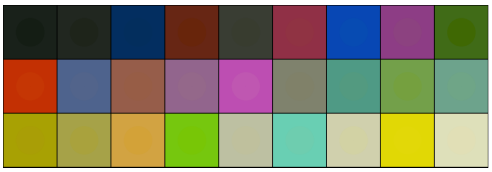

(d) Reflected values - yellow surface

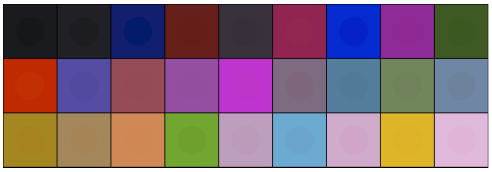

(e) Reflected values - magenta surface

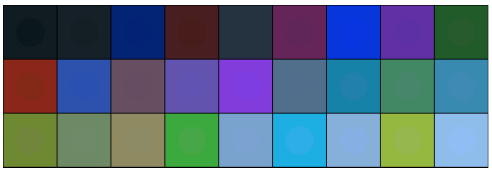

(f) Reflected values - light blue surface

Figure 13: Experiment (c). In (a) the XYZ values of the training set for this set of experiments, measured by the XRITE I1 Pro2, converted into the sRGB color space and gamma corrected (the background of each square); the circles at the center of each square, not always visible, show our estimates. In (b) the set of 27 RGB input triplets to the projector, used to create the test set. In (c) - (f) the XYZ values reflected by the color targets, converted into the sRGB color space. The background of each square shows the ground truth, the circles at the center of each square show our estimates.

References

[BBNS12] BIANCO S., BRUNA A., NACCARI F., SCHETTINI R.: Color space transformations for digital photography exploiting information about the illuminant estimation process. *Journal of the Optical Society of America A 29*, 3 (2012), 374–384. 10

[BBNS13] BIANCO S., BRUNA A., NACCARI F., SCHETTINI R.: Color correction pipeline optimization for digital cameras. *Journal of Electronic Imaging 22*, 2 (2013), 023014. 10

[BGRS07] BIANCO S., GASPARINI F., RUSSO A., SCHETTINI R.: A new method for rgb to xyz transformation based on pattern search optimization. *IEEE Transactions on Consumer Electronics 53*, 3 (2007), 1020–1028. 6

[Bia10] BIANCO S.: Reflectance spectra recovery from tristimulus values by adaptive estimation with metameric shape correction. *Journal of the Optical Society of America A 27*, 8 (2010), 1868–1877. 3

[BS14] BIANCO S., SCHETTINI R.: Error-tolerant color rendering for digital cameras. *Journal of Mathematical Imaging and Vision 50*, 3 (2014), 235–245. 6

[BSV09] BIANCO S., SCHETTINI R., VANNESCHI L.: Empirical modeling for colorimetric characterization of digital cameras. In *Image Processing (ICIP), 2009 16th IEEE International Conference on* (2009), pp. 3469–3472. 2, 8

[CIEa] CIE: *015:2004 Colorimetry, 3rd Edition*. Tech. rep. 3

[CIEb] CIE: *116-1995 Industrial Colour-Difference Evaluation*. Tech. rep. 2, 9

[CIEc] CIE: *142-2001 Improvement to Industrial Colour-Difference Evaluation*. Tech. rep. 2, 9

[Deb98] DEBEVEC P.: Rendering synthetic objects into real scenes: Bridging traditional and image-based graphics with global illumination and high dynamic range photography. In *Proceedings of the 25th Annual Conference on Computer Graphics and Interactive Techniques* (New York, NY, USA, 1998), SIGGRAPH '98, ACM, pp. 189–198. 10

[DHT*00] DEBEVEC P., HAWKINS T., TCHOU C., DUIKER H.-P., SAROKIN W., SAGAR M.: Acquiring the reflectance field of a human face. In *Proceedings of the 27th Annual Conference on Computer Graphics and Interactive Techniques* (New York, NY, USA, 2000), SIGGRAPH '00, ACM Press/Addison-Wesley Publishing Co., pp. 145–156. 1

[DM97] DEBEVEC P. E., MALIK J.: Recovering high dynamic range radiance maps from photographs. In *Proceedings of the 24th Annual Conference on Computer Graphics and Interactive Techniques* (New York, NY, USA, 1997), SIGGRAPH '97, ACM Press/Addison-Wesley Publishing Co., pp. 369–378. 2, 6

[DvGNK99] DANA K. J., VAN GINNEKEN B., NAYAR S. K., KOENDERINK J. J.: Reflectance and texture of real-world surfaces. *ACM Trans. Graph. 18*, 1 (Jan. 1999), 1–34. 1

[FCM*08] FRANCKEN Y., CUYPERS T., MERTENS T., GIELIS J., BEKAERT P.: High quality mesostructure acquisition using specularities. In *CVPR* (2008). 1

[FD97] FINLAYSON G. D., DREW M. S.: Constrained least-squares regression in color spaces. *Journal of Electronic Imaging 6*, 4 (1997), 484–493. 3

[FMH11] FINLAYSON G. D., MACKIEWICZ M., HURLBERT A.: Root-polynomial colour correction. In *Color and Imaging Conference* (2011), vol. 2011, Society for Imaging Science and Technology, pp. 115–119. 6

[Foo97] FOO S.: A gonioreflectometer for measuring the bidirectional reflectance of material for use in illumination computation. In *Thesis 1997 Cornell University* (1997), Cornell University, p. 145. 1

[GCP*09] GHOSH A., CHEN T., PEERS P., WILSON C. A., DEBEVEC P.: Estimating specular roughness and anisotropy from second order spherical gradient illumination. In *Proceedings of the Twentieth Eurographics Conference on Rendering* (Aire-la-Ville, Switzerland, Switzerland, 2009), EGSR'09, Eurographics Association, pp. 1161–1170. 1

[GCP*10] GHOSH A., CHEN T., PEERS P., WILSON C. A., DEBEVEC P.: Circularly polarized spherical illumination reflectometry. *ACM Trans. Graph. 29*, 6 (Dec. 2010), 162:1–162:12. 1, 2

[GGG*16] GUARNERA D., GUARNERA G., GHOSH A., DENK C., GLENCROSS M.: Brdf representation and acquisition. *Computer Graphics Forum 35*, 2 (2016), 625–650. 2, 10

[GHCG17] GUARNERA G. C., HALL P., CHESNAIS A., GLENCROSS M.: Woven fabric model creation from a single image. *ACM Trans. Graph. 36*, 5 (Oct. 2017), 165:1–165:13. 1

[GLS04] GOESELE M., LENSCH H., SEIDEL H.-P.: Validation of color managed 3d appearance acquisition. In *Color and Imaging Conference* (2004), vol. 2004, Society for Imaging Science and Technology, pp. 265–270. 2

[GPDG12] GUARNERA G., PEERS P., DEBEVEC P., GHOSH A.: Estimating surface normals from spherical stokes reflectance fields. In *Computer Vision - ECCV 2012. Workshops and Demonstrations*, Fusiello A., Murino V., Cucchiara R., (Eds.), vol. 7584 of *Lecture Notes in Computer Science*. Springer Berlin Heidelberg, 2012, pp. 340–349. 1, 2

[hdr] University of Southern California, Institute for Creative Technologies, Graphics Lab - HDRShop v3.1. http://gl.ict.usc.edu/HDRShop/index.php. Accessed: 2017-03-21. 3

[HFHD97] HUBEL P., FINLAYSON G., HOLM J., DREW M. S.: Matrix calculations for digital photography. In *Fifth Color Imaging Conference: Color Science, Systems and Applications* (Scottsdale, Arizona, november 1997), pp. 105–111. 3

[HP03] HAN J. Y., PERLIN K.: Measuring bidirectional texture reflectance with a kaleidoscope. *ACM Trans. Graph. 22*, 3 (July 2003), 741–748. 1

[HR76] HSIA J. J., RICHMOND J. C.: Bidirectional reflectometry. part i: A high resolution laser bidirectional reflectometer with results on several optical coatings. *Journal of Reseach of the National Bureau of Standards-A. Physics and Chemistry A 80* (1976), 189–205. 1

[ISO06] ISO: *ISO/17321-1:2006: Graphic technology and photography – Colour characterisation of digital still cameras (DSCs) – Part 1: Stimuli, metrology and test procedures*. Tech. rep., 2006. 2

[ITU15] ITU: *Recommendation ITU-R BT.709-6: Parameter values for the HDTV standards for production and international programme exchange*. Tech. rep., 2015. 2

[JLGS13] JIANG J., LIU D., GU J., SUSSTRUNK S.: What is the space of spectral sensitivity functions for digital color cameras? In *Applications of Computer Vision (WACV), 2013 IEEE Workshop on* (2013), pp. 168–179. 5

[Kaj86] KAJIYA J. T.: The rendering equation. *SIGGRAPH Comput. Graph. 20*, 4 (Aug. 1986), 143–150. 3

[KK08] KIM M. H., KAUTZ J.: Characterization for high dynamic range imaging. *Computer Graphics Forum 27*, 2 (2008), 691–697. 2, 3, 10

[LT97] LEWIS R. M., TORCZON V.: On the convergence of pattern search algorithms. *SIAM J. Optim 7*, 1 (1997), 1–25. 6

[LT00] LEWIS R. M., TORCZON V.: Pattern search methods for linearly constrained minimization. *SIAM J. Optim 10*, 3 (2000), 917–941. 6

[LYL*16] LEGENDRE C., YU X., LIU D., BUSCH J., JONES A., PATTANAIK S., DEBEVEC P.: Practical multispectral lighting reproduction. *ACM Trans. Graph. 35*, 4 (July 2016), 32:1–32:11. 10

[MGW01] MALZBENDER T., GELB D., WOLTERS H.: Polynomial texture maps. In *Proceedings of the 28th Annual Conference on Computer Graphics and Interactive Techniques* (New York, NY, USA, 2001), SIGGRAPH '01, ACM, pp. 519–528. 1

[MMD76] MCCAMY C. S., MARCUS H., DAVIDSON J.: A color-rendition chart. *J. App. Photog. Eng 2*, 3 (1976), 95–99. 2

[MN99] MITSUNAGA T., NAYAR S. K.: Radiometric self calibration. In *Proceedings. 1999 IEEE Computer Society Conference on Computer Vision and Pattern Recognition (Cat. No PR00149)* (1999), vol. 1, p. 380 Vol. 1. 2

[MPBM03] MATUSIK W., PFISTER H., BRAND M., MCMILLAN L.: Efficient isotropic brdf measurement. In *Proceedings of the 14th Eurographics Workshop on Rendering* (Aire-la-Ville, Switzerland, Switzerland, 2003), EGRW '03, Eurographics Association, pp. 241–247. 1, 2

[MPVC03] MARTINEZ-VERDU F., PUJOL J., VILASECA M., CAPILLA P.: Characterization of a digital camera as an absolute tristimulus colorimeter. In *Society of Photo-Optical Instrumentation Engineers (SPIE) Conference Series* (Jan. 2003), Eschbach R., Marcu G. G., (Eds.), vol. 5008 of *Society of Photo-Optical Instrumentation Engineers (SPIE) Conference Series*, pp. 197–208. 4, 8, 10

[MSHD15] MENG J., SIMON F., HANIKA J., DACHSBACHER C.: Physically meaningful rendering using tristimulus colours. In *Proceedings of the 26th Eurographics Symposium on Rendering* (Aire-la-Ville, Switzerland, Switzerland, 2015), EGSR '15, Eurographics Association, pp. 31–40. 3

[MVPC02] MARTINEZ-VERDU F., PUJOL J., CAPILLA P.: Calculation of the color matching functions of digital cameras from their complete spectral sensitivities. *Journal of Imaging Science and Technology 46*, 1 (2002), 15–25. 4

[MWL*99] MARSCHNER S. R., WESTIN S. H., LAFORTUNE E. P., TORRANCE K. E., GREENBERG D. P.: Image-based brdf measurement including human skin. In *Rendering Techniques 99*. Springer, 1999, pp. 131–144. 1, 2

[NDM05] NGAN A., DURAND F., MATUSIK W.: Experimental analysis of brdf models. In *Proceedings of the Sixteenth Eurographics Conference on Rendering Techniques* (Aire-la-Ville, Switzerland, Switzerland, 2005), EGSR'05, Eurographics Association, pp. 117–126. 1, 2

[NM00] NAYAR S. K., MITSUNAGA T.: High dynamic range imaging: spatially varying pixel exposures. In *Proceedings IEEE Conference on Computer Vision and Pattern Recognition. CVPR 2000 (Cat. No.PR00662)* (2000), vol. 1, pp. 472–479 vol.1. 2

[NRH*77] NICODEMUS F., RICHMOND J., HSIA J., GINSBERG I., LIMPERIS T.: Geometrical considerations and nomenclature for reflectance, natl. *Bur. Stand. Rep., NBS MN-160* (1977). 1

[RMS*08] RUMP M., MÜLLER G., SARLETTE R., KOCH D., KLEIN R.: Photo-realistic rendering of metallic car paint from image-based measurements. *Computer Graphics Forum 27*, 2 (Apr. 2008), 527–536. 1, 2

[RPAC17] RHEE T., PETIKAM L., ALLEN B., CHALMERS A.: Mr360: Mixed reality rendering for 360○ panoramic videos. *IEEE Transactions on Visualization and Computer Graphics 23*, 4 (April 2017), 1379–1388. 10

[RPG16] RIVIERE J., PEERS P., GHOSH A.: Mobile surface reflectometry. *Computer Graphics Forum 35*, 1 (2016), 191–202. 1

[RSH*99] RUECKERT D., SONODA L. I., HAYES C., HILL D. L. G., LEACH M. O., HAWKES D. J.: Nonrigid registration using free-form deformations: application to breast mr images. *IEEE Transactions on Medical Imaging 18*, 8 (Aug 1999), 712–721. 8

[RWPD05] REINHARD E., WARD G., PATTANAIK S., DEBEVEC P.: *High Dynamic Range Imaging: Acquisition, Display, and Image-Based Lighting (The Morgan Kaufmann Series in Computer Graphics)*. Morgan Kaufmann Publishers Inc., San Francisco, CA, USA, 2005. 2

[Sha03] SHARMA G.: *Digital Color Imaging Handbook*. CRC Press, Inc., Boca Raton, FL, USA, 2003. 3, 4

[TS67] TORRANCE K. E., SPARROW E. M.: Theory for off-specular reflection from roughened surfaces. *JOSA 57*, 9 (1967), 1105–1112. 1

[WEV02] WARD G., EYDELBERG-VILESHIN E.: Picture perfect rgb rendering using spectral prefiltering and sharp color primaries. In *Proceedings of the 13th Eurographics Workshop on Rendering* (Aire-la-Ville, Switzerland, Switzerland, 2002), EGRW '02, Eurographics Association, pp. 117–124. 3

[WS82] WYSZECKI G., STILES W. S.: *Color science: Concepts and Methods, Quantitative Data and Formulae*, vol. 8. Wiley, New York, NY, USA, 1982. 2, 9